Magnetic states of the two-leg-ladder alkali metal iron selenides $A\mathrm{Fe_2Se_3}$

Qinlong Luo,[1,2] Andrew Nicholson,[1,2] Julián Rincón,[1,2] Shuhua Liang,[1,2] José Riera,[3] Gonzalo Alvarez,[4] Limin Wang,[5] Wei Ku,[5,6] German D. Samolyuk,[2] Adriana Moreo,[1,2] and Elbio Dagotto[1,2]

[1]*Department of Physics and Astronomy, The University of Tennessee, Knoxville, Tennessee 37996, USA*

[2]*Materials Science and Technology Division, Oak Ridge National Laboratory, Oak Ridge, Tennessee 37831-6138, USA*

[3]*Instituto de Física Rosario, Universidad Nacional de Rosario, 2000-Rosario, Argentina*

[4]*Computer Science and Mathematics Division and Center for Nanophase Materials Sciences, Oak Ridge National Laboratory, Oak Ridge, Tennessee 37831, USA*

[5]*Condensed Matter Physics and Materials Science Department, Brookhaven National Laboratory, Upton, New York 11973, USA*

[6]*Physics Department, State University of New York, Stony Brook, New York 11790, USA*

(Received 14 May 2012; revised manuscript received 2 October 2012; published 8 January 2013)

Recent neutron scattering experiments addressing the magnetic state of the two-leg-ladder selenide compound $\mathrm{BaFe_2Se_3}$ have unveiled a dominant spin arrangement involving ferromagnetically ordered 2×2 iron superblocks, that are antiferromagnetically coupled among them (the "block-AFM"state). Using the electronic five-orbital Hubbard model first-principles techniques to calculate the electronic hopping amplitudes between irons, and the real-space Hartree-Fock approximation to handle the many-body effects, here it is shown that the exotic block-AFM state is indeed stable at realistic electronic densities close to $n \sim 6.0$. Another state with parallel spins along the rungs and antiparallel along the legs of the ladders (the "CX" state) is close in energy. This state becomes stable in other portions of the phase diagrams, such as with hole doping, as also found experimentally via neutron scattering applied to $\mathrm{KFe_2Se_3}$. In addition, the present study unveils other competing magnetic phases that could be experimentally stabilized by varying either n chemically or the electronic bandwidth by pressure. Similar results were obtained using two-orbital models, studied here via Lanczos and density-matrix renormalization group (DMRG) techniques. A comparison of the results obtained with the realistic selenides hopping amplitudes for $\mathrm{BaFe_2Se_3}$ against those found using the hopping amplitudes for pnictides reveals several qualitative similarities, particularly at intermediate and large Hubbard couplings.

DOI: 10.1103/PhysRevB.87.024404 PACS number(s): 74.70.Xa, 74.20.Rp, 71.10.Fd, 75.10.Lp

I. INTRODUCTION

The study of Fe-based superconductors[1–3] continues to unveil fascinating new discoveries at a fast pace. Among the most recent developments is the report of superconductivity in the intercalated iron selenides $\mathrm{K_{0.8}Fe_{2-x}Se_2}$ and $\mathrm{(Tl,K)Fe_{2-x}Se_2}$.[4] In addition, at the special composition $\mathrm{K_{0.8}Fe_{1.6}Se_2}$ with the iron vacancies in a $\sqrt{5} \times \sqrt{5}$ arrangement, neutron scattering studies[5,6] of this (insulating) compound have revealed an unusual magnetic order. This magnetic state involves 2×2 iron blocks with their four spins ferromagnetically ordered, large ordering temperatures, and concomitant large magnetic moments $\sim 3.3\ \mu_B$/Fe. The 2×2 blocks are antiferromagnetically coupled among them. Phase separation tendencies have also been reported in this type of insulator.[7] Photoemission experiments for $\mathrm{(Tl, K)Fe_{1.78}Se_2}$ revealed a Fermi surface with only electronlike pockets at wave vectors $(\pi,0)$ and $(0,\pi)$,[8] showing that the Fermi surface nesting of hole and electron pockets is not sufficient to understand these materials.[2]

The developments described above suggest that progress in the understanding of chalcogenides could be made if the iron spins are arranged differently than in the nearly square lattice geometry of the FeSe layers. For this reason considerable interest was generated by recent studies[9–14] of $\mathrm{BaFe_2Se_3}$ (the "123" compound) since this material contains chains made of $[\mathrm{Fe_2Se_3}]^{2-}$ building blocks separated by Ba. These effective two-leg iron ladders in $\mathrm{BaFe_2Se_3}$ are cutouts of the layers of edge-sharing $\mathrm{FeSe_4}$ tetrahedra normally found in layered chalcogenides. Each double chain consists of pairs of iron atoms (the "rungs") located one next to the other forming a one-dimensional arrangement perpendicular to those rungs, defining indeed a two-leg ladder structure. In the context of the Cu-oxide high-T_c superconductors, spin-1/2 two-leg ladders have also been much studied because of their unusual spin gap, induced by the ladder geometry. The Cu-oxide-ladder spin state is dominated by rung spin singlets, and a tendency to superconduct upon doping.[15,16] In particular, the compound $\mathrm{SrCu_2O_3}$ is the Cu-based analog of $\mathrm{BaFe_2Se_3}$.[17]

A recent remarkable development that increases the relevance of the iron-based ladders is the following. The preparation of a single layer of alkali-doped FeSe with the geometry of weakly coupled two-leg ladders was recently reported in Ref. 18, where it was also argued that this ladder system is superconducting based on the presence of a gap in the local density of states. These results suggest that Fe-based ladders provide a simple playground where even superconductivity can be explored, increasing the similarities with the Cu-oxide ladders that are also superconducting.[17]

$\mathrm{BaFe_2Se_3}$ is an insulator, with a resistivity displaying an activation energy between $\Delta \sim 0.13$ eV (Ref. 14) and $\Delta \sim 0.178$ eV (Ref. 11). The 123-ladder compound has long-range antiferromagnetic (AFM) order at $\sim$250 K, with low-temperature magnetic moments $\sim 2.8\ \mu_B$, and it displays short-range AFM correlations at higher temperatures (in particular $\xi \sim 35$Å at room T).[10–12] Upon cooling, the magnetic order presumably settles along the ladder directions first, and then weaker interladder interactions establish the long-range order. Neutron diffraction studies[10,14] reported a dominant magnetic order at low T involving blocks of four iron atoms with their moments aligned, coupled antiferromagnetically along

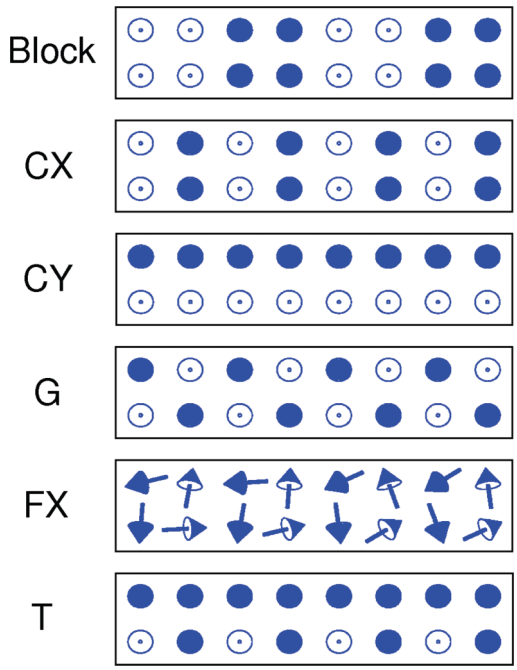

FIG. 1. (Color online) Magnetic states observed in the phase diagrams of the multiorbital Hubbard models used in this study, employing the geometry of a two-leg ladder.

the ladder direction (Fig. 1, top state). This state is sometimes dubbed the plaquette state, but here it will be referred to as the "block-AFM" state or just "Block". The ferromagnetic 2×2 building blocks present in the block-AFM state of the ladders are the same blocks reported before in $K_{0.8}Fe_{1.6}Se_2$, with the iron vacancies in the $\sqrt{5} \times \sqrt{5}$ distribution. When the 123-ladder material is doped with K as in $Ba_{1-x}K_xFe_2Se_3$, experimentally it is known that the magnetic state evolves from the block-AFM state, through a spin glass, eventually arriving for KFe_2Se_3 to the spin state labeled "CX" also displayed in Fig. 1, where the spins in the same rung are coupled ferromagnetically but they are antiferromagnetically ordered in the long ladder direction.[13] Note that in $BaFe_2Se_3$ the valence of Fe is expected to be $2+$, if those of Ba and Se are $+2$ and -2, respectively, giving an electronic density $n = 6.0$. But in KFe_2Se_3, K has valence $+1$, thus rendering the average valence of Fe to be $+2.5$, that corresponds to an electronic density $n = 5.5$.

In the present paper, results for multiorbital Hubbard models are reported. The lattice distortions[10,11] are partially taken into account via the hopping amplitudes, as described below. However, part of our results presented in the following sections show that even without lattice distortions the 2×2 block-AFM state is stable in regions of the phase diagrams that are constructed by varying the on-site Hubbard repulsion U, the Hund coupling J_H, and the electronic density n.[19] In other words, our most important result is that several models, studied with several approximations, systematically contain the block-AFM state as a robust phase in the phase diagram. Moreover, the other recently observed[13] CX state is also found in the resulting phase diagrams. Several competing states that could be stabilized in related compounds or under pressure or via chemical doping are also discussed.

The present study is carried out mainly using the Hartree-Fock approximation for the five-orbital Hubbard model, employing both a set of hopping amplitudes that are deduced from first-principles techniques applied to the selenide 123 ladders, as explained below, and also an "old" set of hopping that was previously employed in layered pnictides. The purpose of using two sets of hoppings is to gauge how sensitive the results are with regard to modifications in those hopping amplitudes. In addition, our results for pnictide hoppings can be considered predictions in case two-leg ladder pnictides are synthesized in the future. Results for a reduced two-orbital Hubbard model using Lanczos[20] and the density-matrix renormalization group (DMRG)[21] techniques are also presented here, also for two sets of hoppings. Overall, the two phases observed experimentally in neutron scattering, the block-AFM and the CX states, are stable in regions of the phase diagram centered at the realistic Hund coupling $J_H/U = 0.25$. With regard to phase diagrams, gaps, magnetic moments, and competing states, a reasonable qualitative agreement is found between the two different hopping sets, and for the different number of orbitals considered in our effort. Studies of the spin-fermion two-orbital model[22] using Monte Carlo simulations[23] also provide a phase diagram compatible with those of the Hubbard models.

II. FIVE-ORBITAL HUBBARD MODEL, HOPPING AMPLITUDES, AND METHODS

In this section, the focus will be on the derivation of the hopping amplitudes needed for the five-orbital Hubbard model and in providing details of the real-space Hartree-Fock technique employed. The models used in this paper have all been extensively discussed before, thus details will not be repeated. In particular, the five-orbital Hubbard model is explicitly defined in Ref. 24. With regard to the hopping amplitudes for the 123-ladder compounds, here they have been calculated using first-principles techniques, as explained below. These hoppings will be refereed to as the selenide hoppings in the rest of the paper.[25] For completeness, results using the hoppings corresponding to layered pnictides[26] will also be used, and the results compared with one another. While the data gathered with the realistic selenide hoppings are our most important set of results, contrary to naive expectations it will be shown that a reasonable agreement is observed between these two *a priori* quite different sets of hopping amplitudes, at least at a qualitative level. The electronic density of main interest is, in principle, $n \sim 6.0$ (i.e., 6 electrons/Fe), thus our efforts are centered at this density, but some results varying n are shown below as well (or verbally described). As explained before, the on-site intraorbital Hubbard repulsion is U, the Hund coupling is J_H, and the interorbital repulsion U' is assumed to satisfy $U' = U - 2J_H$. Ladders of sizes $2 \times L$ ($L = 4, 8, 16, 32$) were studied, and size effects were found to be mild. Periodic (open) boundary conditions are used along the chain (rung) direction.

The selenides hopping amplitudes for the 123 ladders were obtained via a first-principles density functional theory calculation of the nonmagnetic normal state. The calculation was conducted using the WIEN2K implementation of the full potential linearized augmented plane wave method in the local density approximation.[27] The k-point mesh was taken to be

TABLE I. Hopping matrices for the $BaFe_2Se_3$ material obtained from a tight-binding Wannier function analysis of the first-principles results (in eV units). The matrices are written in the orbital basis $\{d_{z^2}, d_{x^2-y^2}, d_{yz}, d_{xz}, d_{xy}\}$ for the on-site energy and interorbital hopping (t^{OnSite}), nearest-neighbors hoppings (t^{NN}, both along the rungs and the legs) and next-nearest-neighbors hoppings (t^{NNN}). The long (short) direction of the ladder is oriented along the y (x) axis. The convention for the iron site labels is in Fig. 2. Note that each 5×5 matrix in this table should be considered as the hopping matrix to move from one iron to another as indicated. For a given Fe-Fe bond, the full matrix that includes both the back and forth processes for the hopping is of size 10×10 and it consist of a 5×5 matrix of this table in a nondiagonal block, the transpose in the other nondiagonal 5×5 block, and the on-site matrix (top of this table) in both diagonal blocks.

Matrix	$BaFe_2Se_3$
t^{OnSite}	$\begin{pmatrix} -0.4604 & -0.0617 & 0.0534 & -0.0345 & -0.0178 \\ -0.0617 & -0.5947 & -0.0851 & 0.0371 & 0.0169 \\ 0.0534 & -0.0851 & -0.0719 & -0.0030 & 0.0165 \\ -0.0345 & 0.0371 & -0.0030 & -0.1669 & 0.0286 \\ -0.0178 & 0.0169 & 0.0165 & 0.0286 & -0.1632 \end{pmatrix}$
$t^{\text{NN}}_{\text{leg},1\to 8}$	$\begin{pmatrix} -0.0807 & -0.3276 & -0.0139 & 0.2734 & 0.0456 \\ -0.3276 & -0.2875 & -0.0702 & 0.2661 & 0.0228 \\ 0.0139 & 0.0702 & -0.1477 & -0.0531 & 0.2714 \\ 0.2734 & 0.2661 & 0.0531 & -0.2733 & 0.0373 \\ -0.0456 & -0.0228 & 0.2714 & -0.0373 & -0.0397 \end{pmatrix}$
$t^{\text{NN}}_{\text{leg},1'\to 8}$	$\begin{pmatrix} 0.0497 & -0.2674 & 0.0187 & -0.1186 & -0.0738 \\ -0.2674 & -0.3943 & -0.0388 & -0.3449 & -0.0195 \\ -0.0187 & 0.0388 & -0.0580 & 0.0199 & -0.2689 \\ -0.1190 & -0.3449 & -0.0199 & -0.3107 & -0.0147 \\ 0.0738 & 0.0195 & -0.2689 & 0.0147 & -0.1343 \end{pmatrix}$
$t^{\text{NN}}_{\text{rung},8\to 7}$	$\begin{pmatrix} -0.0421 & 0.2853 & -0.1718 & -0.0162 & 0.0055 \\ 0.2853 & -0.3801 & 0.3311 & 0.0411 & 0.0098 \\ -0.1718 & 0.3311 & -0.2881 & -0.0115 & -0.0259 \\ -0.0162 & 0.0411 & -0.0115 & -0.0058 & -0.2303 \\ 0.0055 & 0.0098 & -0.0259 & -0.2303 & -0.0153 \end{pmatrix}$
$t^{\text{NN}}_{\text{rung},1\to 2'}$	$\begin{pmatrix} -0.0421 & 0.2853 & 0.1718 & -0.0162 & -0.0055 \\ 0.2853 & -0.3801 & -0.3311 & 0.0411 & -0.0098 \\ 0.1718 & -0.3311 & -0.2881 & 0.0115 & -0.0259 \\ -0.0162 & 0.0411 & 0.0115 & -0.0058 & 0.2303 \\ -0.0055 & -0.0098 & -0.0259 & 0.2303 & -0.0153 \end{pmatrix}$
$t^{\text{NNN}}_{2\to 8}$	$\begin{pmatrix} -0.0185 & 0.0054 & 0.1140 & 0.0893 & -0.0721 \\ -0.0159 & -0.0379 & -0.0661 & 0.0603 & -0.0118 \\ -0.1483 & 0.0837 & 0.2117 & 0.0843 & 0.0679 \\ -0.1442 & -0.0490 & 0.0801 & 0.1823 & 0.0559 \\ -0.0879 & -0.0017 & -0.0304 & -0.0529 & 0.0644 \end{pmatrix}$
$t^{\text{NNN}}_{2'\to 8}$	$\begin{pmatrix} -0.0185 & 0.0054 & -0.1140 & 0.0893 & 0.0721 \\ -0.0159 & -0.0379 & 0.0661 & 0.0603 & 0.0118 \\ 0.1483 & -0.0837 & 0.2117 & -0.0843 & 0.0679 \\ -0.1442 & -0.0490 & -0.0801 & 0.1823 & -0.0559 \\ 0.0879 & 0.0017 & -0.0304 & 0.0529 & 0.0644 \end{pmatrix}$

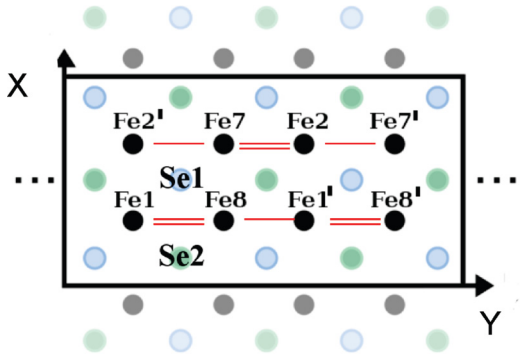

FIG. 2. (Color online) Label convention of the iron sites used in Table I, adapted from Fig. 1(b) of Ref. 10. The single and double lines along the y axis denote two different lattice spacings, with specific numbers taken from Ref. 10. The two selenium sites denote locations above and below the plane defined by the iron ladder.

$7 \times 15 \times 19$. The lattice constants were taken from Ref. 10. Table I shows the hopping parameters calculated by representing the resulting self-consistent Kohn-Sham Hamiltonian with low-energy ($[-2.5,2]$ eV) symmetry-respecting Wannier functions[28] with strong Fe-d symmetry. Since the influence of the As-p orbitals are integrated into the tail of the Wannier functions, the parameters correspond to an effective iron-only model with five orbitals per iron. The staggered location of the selenium atoms, above and below the plane defined by the Fe atoms, is taken into account in the calculation. For a similar discussion in the context of the three orbital model, see Ref. 29. Note also that Table I contains the hoppings that are needed for the full description of the system, based on the iron locations in Fig. 2. Other hoppings are all identical to one of those shown in Table I. For instance, the hopping matrix from Fe2 to Fe7 is the same as the hopping matrix from Fe1 to Fe8 in Table I; the hopping matrix from Fe1 to Fe7 is the same as the hopping matrix from Fe2 to Fe8, etc.

In addition, and for completeness, the hopping parameters of Ref. 26 obtained for pnictide compounds were also used in our studies. The goal was to test our conclusions against reasonable modifications in the hoppings. Several aspects of our results were found to be qualitatively similar for the two sets of hoppings although, of course, quantitatively there are substantial differences.

The five-orbital Hubbard model is studied here using the real-space Hartree-Fock (HF) approximation, taking into account the staggered location of the Se atoms via the proper hopping amplitudes. Recently, the same method was successfully employed in the analysis of $K_{0.8}Fe_{1.6}Se_2$ and other systems.[30,31] A real-space approach, where all the HF expectation values that need to be found self-consistently are assumed independent from site to site, allows for the system to select spontaneously the state that minimizes the HF energy, reducing the bias into the calculations. The HF expectation values are obtained by an iterative process that reduces the energy until convergence.[32] The results shown below have been computationally obtained by two procedures: (i) using as initial configurations the states in Fig. 1 and then comparing energies after convergence, or (ii) starting with totally random values and analyzing the spin order particularly

at short distances. Procedure (ii), computationally demanding due to the large number of iterations needed, sometimes allows for the identification of "unexpected" phases [that then become part of (i)] and also to confirm the results of procedure (i).

III. RESULTS FOR THE FIVE-ORBITAL HUBBARD MODEL

A. Phase diagrams and the block-AFM phase

The main results of the present HF study of the five-orbital Hubbard model are shown in Fig. 3, where the phase diagrams varying U/W and J_H/U are presented using both the realistic selenides hoppings for the 123 ladders as well as the pnictides hoppings for comparison. The bandwidth

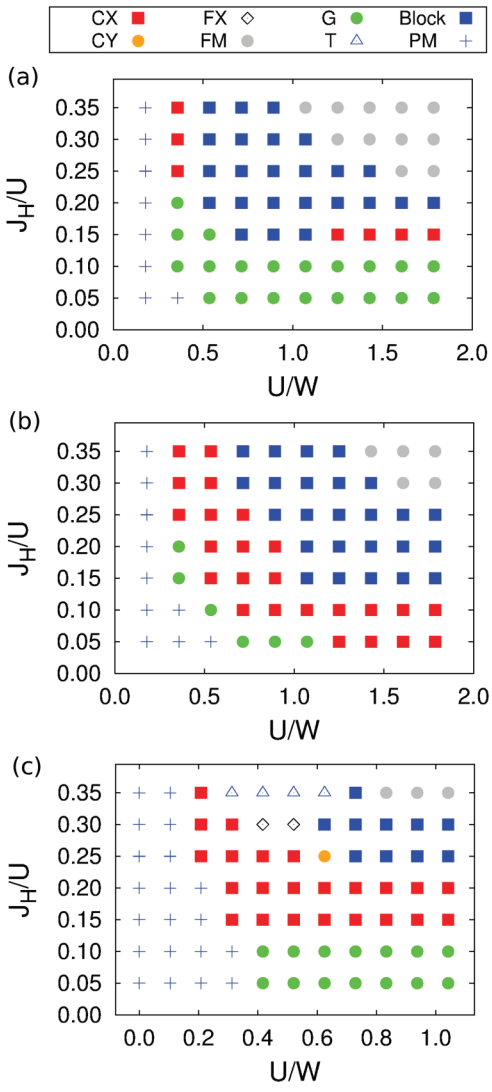

FIG. 3. (Color online) Phase diagram of the five-orbital Hubbard model in the real-space HF approximation. The label convention for the phases is in the upper inset and also in Fig. 1. PM denotes a paramagnetic state. (a) Results for a 2×16 cluster, using the selenides hopping amplitudes for the 123 ladders, and at electronic density $n = 6.0$. (b) Same as (a) but for electronic density $n = 5.75$. (c) Results for a 2×32 cluster, using the pnictides hopping amplitudes, and working at electronic density $n = 6.0$.

W of the five-orbital Hubbard model is ∼2.8 eV for the selenides hoppings, while for the pnictides hoppings it is ∼4.8 eV.[26] In all cases, Figs. 3(a)–3(c) show the remarkable result that the block-AFM phase found in neutron experiments for the 123 ladders[10,14] becomes stable in a robust region of the phase diagram. This is interesting since the 2×2 blocks in ladders are not as clearly geometrically defined as in the $\sqrt{5} \times \sqrt{5}$ iron-vacancies arrangements, where each of the plaquettes of the tilted square lattice of those iron vacancies already contains a 2×2 block inside. In our two-leg ladders, on the other hand, the ferromagnetic (FM) blocks do emerge spontaneously in the calculations described here and in experiments as well. As explained before, the present results were confirmed using unbiased random starting configurations for the HF expectation values and an iterative procedure for convergence. By this procedure, the stability of the block-AFM state was indeed tested at several points of the phase diagram. Moreover, it is interesting that the region of stability includes the realistic ratio $J_H/U = 0.25$, found before to correspond to the "physical region" where a good agreement theory experiment was observed for the pnictides.[24,33]

With regard to the actual value of U/W, note that the block-AFM phase is stabilized starting at $U/W \sim 0.5 - 0.6$ for the selenides hoppings [Figs. 3(a) and 3(b)] and at $U/W \sim 0.6$ for the pnictide hoppings [Fig. 3(c)]. This is similar to the value ∼0.52 reported for $K_{0.8}Fe_{1.6}Se_2$ in Ref. 30 using similar techniques. The critical U/W quoted above are slightly larger than the $U/W \sim 0.31$ needed for the pnictides in the planar geometry of the "1111" and "122" materials to form the C-type AFM state,[24,33] but note that in our present results magnetic order in the CX channel (the analog of the C-type AFM phase) is reached at $U/W \sim 0.3$ in good agreement with those previous investigations. Considering that it is the block-AFM state that is found experimentally for the 123-ladder selenides, this suggests that these selenides are more strongly correlated than pnictides and their ratios of U/W are roughly $0.5/0.3 = 1.66$. Note also that the actual values of U/W are still smaller than 1, the ratio often considered as the boundary of the strong coupling limit, implying that the selenide ladders are still "intermediate" coupling compounds.[2] However, the HF approximation favors ordered states, and including quantum fluctuations the U/W needed to stabilize the block-AFM phase may exceed 1. On the other hand, note also that results in real ladders may be influenced by the presence of a robust electron-lattice coupling (mentioned in Refs. 10 and 11) that may render stable the block-AFM phase even at values of U/W not as large as needed for its stabilization when based entirely on an electronic mechanism. In spite of these caveats, it is clear that even with lattice distortions incorporated the presence of sizable electronic correlations appears to be important to stabilize the block-AFM state.

In the block-AFM phase found in our study the magnetic moment per Fe is large and close to saturation. More specifically, it is ∼4.0 μ_B for the selenides hoppings and ∼3.9 μ_B for the pnictides hoppings, with small variations caused by the selection of specific values of U. The difference with the experimental result[10] ∼2.8 μ_B may be caused by the absence of fluctuations in the HF approximation,[34] or by the neglect of lattice distortions in our effort, as already discussed. But at least qualitatively the large value of the magnetic moment, as

compared with the relatively small moments reported in some layered pnictides is here properly reproduced.

In the present Hartree-Fock effort, square 8×8 clusters have also been studied to address the coupling between ladders in the direction perpendicular to the legs. In practice, a weak interladder coupling was introduced by multiplying by a small factor $\alpha = 0.1$ all the hoppings connecting sites belonging to different individual 2×8 ladders (thus the 8×8 cluster has four of these two-leg ladders). Other values of (small) α were used and the results were all similar. The main result (not shown) is that the phase diagrams using the 8×8 clusters are virtually identical to those found for the individual two-leg ladders, for both sets of hoppings, with the only interesting detail that the weak coupling between the ladders establishes an effective antiferromagnetic coupling between them, as found experimentally.[10]

B. The CX phase and other competing states

It is important to remark that in all Figs. 3(a)–3(c) there are several other magnetic states in addition to the block-AFM state. In particular, the CX phase found experimentally in hole-doped ladders[13] also occupies a robust region of the phase diagram, and it is located next to the block-AFM phase for both the selenides 123-ladder hoppings as well as the pnictide hoppings, at the electronic densities investigated in Fig. 3. Its region of stability includes areas with smaller or similar values for U/W than those where the block-AFM state is stable. Our investigations varying n reveal that this phase is stable in a broad region of parameter space, including the $n = 5.5$ electronic density corresponding to KFe_2Se_3,[13] indicating once again a good agreement between calculations and experiments. In fact, Fig. 3(b) shows that the CX state is more stable at electronic density $n = 5.75$ than at $n = 6.0$, compatible with experiments. The CX state can be considered closely related to the C-AFM state of layered pnictides with the wave vector $(\pi,0)$, thus its stability particularly close to the PM state should not be too surprising.

Varying U/W and J_H/U, phases that have not been observed experimentally for the two-leg ladders become stable. For instance, when the Hund coupling is small compared with U, a G-type antiferromagnetic state is found, with staggered magnetic order. In the other extreme of magnetic order, ferromagnetism is observed in a small region of parameter space for a sufficiently large U and Hund couplings, for both sets of hoppings. The qualitative tendency from G to CX to block-AFM to FM with increasing J_H/U at robust U/W goes together with the tendency to FM order in the vicinity of each iron atom: for the G state the three NN links are AFM, for the CX state two are AFM and one is FM, for the block-AFM state two are FM and one AFM, and of course for the full FM state all NN links are FM.

Small "islands" of other states are also present in the phase diagram corresponding to the pnictides hoppings, including the CY state which is another relative of the C-AFM state of the pnictides, as well as the flux and T states (see Fig. 1 for the spin arrangement corresponding to these states). But it is clear that the block-AFM, CX, G, FM, and PM states dominate the phase diagrams.

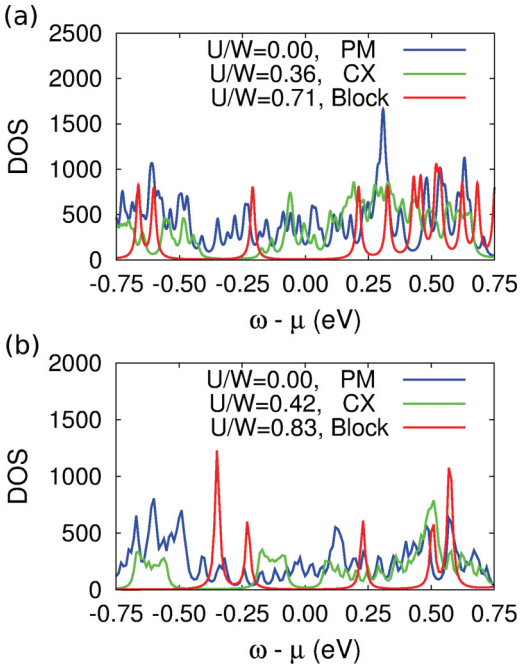

FIG. 4. (Color online) Density of states of the five-orbital Hubbard model (in the HF approximation), at $J_H/U = 0.25$, and the values of U/W indicated. The type of phase state corresponding to each value of U/W is also indicated. (a) corresponds to the selenides hoppings for the 123-ladder compound and electronic density $n = 6.0$. The bandwidth W in this case is $\sim$2.8 eV. (b) corresponds to the pnictides hoppings, for comparison. The electronic density is $n = 6.0$, and the bandwidth W is $\sim$4.8 eV. In both cases, the small oscillations at $U/W = 0$ and in the CX phase are caused by size effects in the long direction of the 2×16 or 2×32 clusters used and the intrinsic small size in the rung direction.

C. Density of states

The density of states (DOS) of the block-AFM state for both the cases of the selenides 123-ladder hoppings and the pnictides hoppings are shown in Fig. 4 for representative couplings. The presence of a gap at the chemical potential for the block-AFM state and for both hoppings indicates an insulating state, in agreement with experiments. While the values of the gap for the block-AFM state ($\Delta \sim 0.40$ eV and $\Delta \sim 0.45$ eV for the selenides and pnictides hoppings, respectively) are larger than reported experimentally,[11,14] the qualitative trends are correct. Further improvement with experiments can be achieved by better fine tuning U/W and J_H/U, by adding effects arising from the three dimensionality of the problem, incorporating other lattice distortions, etc.

Another detail that merits a comment is that the CX phase, being closer in the phase diagrams to the PM state than the block-AFM state is, has a metallic or weakly insulating character that depends on specific details such as the value of U/W. At a fixed J_H/U such as 0.25, the metal-insulator transition seems to occur within the CX phase.

IV. RESULTS FOR THE TWO-ORBITAL HUBBARD MODEL

The results obtained via the HF approximation to the five-orbital Hubbard model can be further analyzed, at least

qualitatively, by studying models with less orbitals but using computational techniques beyond the mean-field approximation. Consider for instance the two-orbital Hubbard model employing the d_{xz} and d_{yz} orbitals. This model can be studied exactly in small clusters, via the Lanczos algorithm,[20] or via DMRG techniques. Here, in the first part of the study using the two-orbital model, the hoppings originally developed for pnictides will be used, but then in the second part a set of hoppings derived from the five-orbital hoppings of the ladder selenides will be employed. For details about the model, particularly the hoppings for the pnictides case, and for the technical aspects of the implementation of the Lanczos technique to multiorbital models see Refs. 35–37. A phase diagram can be constructed by calculating the spin-structure factor $S(q_x,q_y)$, and focusing on the wave vector that maximizes this quantity. In particular, if $S(q_x,q_y)$ is maximized at (0,0) then the state is considered ferromagnetic, if maximized at $(\pi,0)$ it is CX, if at $(0,\pi)$ it is CY, and if at $(\pi/2,0)$ it is the block-AFM state. Before providing the results, it is important to clarify that the discussion involving two orbitals is *qualitative* at best. In fact, the two-orbitals model version of the five-orbitals model derived here from first principles provides only a limited fit of the Fermi surface. However, it will be shown that in spite of this quantitative issues, the crude two-orbitals model used here do present the block-AFM and CX states in the phase diagrams, showing that, within reason, their presence does not depend on details of the hopping amplitudes.

A. Lanczos and pnictides hoppings

By the procedure described above, the results in Fig. 5(a) were obtained using the Lanczos method on a 2×4 lattice, employing the original hopping amplitudes of the two-orbital model for the pnictides. At half-filling $n=2.0$, which is the analog of $n=6.0$ for five orbitals, the CX state, one of the states observed in neutron scattering for ladders,[13] dominates. Increasing the electronic density n, the block-AFM state (the other state reported experimentally)[10] is also stabilized, while decreasing n the CY state (this state has not been reported experimentally yet) becomes the ground state. While a quantitative agreement with the five-orbital model results should not be expected, it is still reassuring that some of the main tendencies are similar when using two and five orbitals. These common aspects are: the block-AFM state is stable at a robust U/W, the CX state dominates a large fraction of the phase diagram, and other states appear as competing alternatives. The reduction from five to two orbitals preserves the essence of the problem, at least qualitatively and at the electronic densities of the parent compounds. Note also that the U/W needed to stabilize the block-AFM phase is approximately 1, namely larger than in the five-orbitals HF analysis. As explained before, the quantum fluctuations considered in the Lanczos calculation could move the critical U/W to larger values than in the mean-field approximation highlighting the need to include correlation effects. However, since other factors such as finite-size effects in Lanczos could influence on the actual values of the critical couplings, this conclusion should be considered only as qualitative. Moreover, note that the comparison between two- and five-orbitals is also

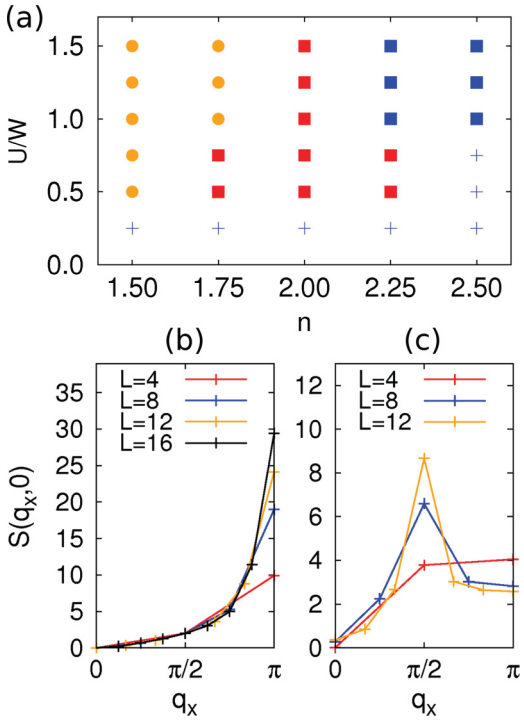

FIG. 5. (Color online) (a) Phase diagram of the two-orbital Hubbard model studied with the Lanczos method on a 2×4 cluster, and at $J_H/U=0.25$. Shown are results varying U/W ($W=12$ eV, see Ref. 35) and the number of total electrons N as 12, 14, 16 ($n=2$), 18, and 20. The assignments of the many phases are decided based on the dominant peak in the spin structure factor. The color convention is as in Fig. 3. (b) DMRG results showing the dominance of the CX state $(\pi,0)$ with increasing L in the spin structure factor $S(q_x,0)$ using $2\times L$ clusters at $U/W=0.83$, $J_H/U=0.25$, and $n=2$. (c) Same as (b) but for the block-AFM state $(\pi/2,0)$, at $U/W=0.83$, $J_H/U=0.25$, and $n=2.5$. The hoppings used in all panels are those of the pnictides (Ref. 26).

only qualitative since, for instance, working at fixed J_H/U the phase diagram of Fig. 3 at $n=6.0$ contains the block-AFM phase at a large enough U/W, while the phase diagram of Fig. 5(a) at $n=2.0$ only has one magnetically ordered state, the CX state. Another discrepancy is the dominance of the CY state for n less than 2.0, feature that is not observed in a five-orbitals context. Thus, the results of both models are certainly not in one-to-one correspondence.

B. DMRG and pnictides hoppings

This same two-orbital Hubbard model was also studied using DMRG techniques.[21] Open boundary conditions were employed in both directions, and typically $m=450$ states and 20 sweeps were used. The energy difference between the last two DMRG sweeps was 10^{-5}. The results are in Figs. 5(b) and 5(c). In Fig. 5(b), the spin structure factor is shown varying L using a $2\times L$ cluster with $L=4$, 8, 12, and 16, at $n=2$, and fixed J_H/U and U/W. In this case, the CX state dominates,[38] as found with the Lanczos technique. In Fig. 5(c), the spin structure factor is shown at $n=2.5$, $J_H/U=0.25$, intermediate coupling $U/W=0.83$, and three cluster sizes showing that in this regime the block-AFM state

TABLE II. Set of hopping matrices for the two-orbital model corresponding to the 123-ladder compound (in eV units), obtained from the selenides set of hoppings for these materials using the five-orbital model. The matrices are written in the orbital basis $\{d_{xz}, d_{yz}\}$ along the x, y, $x+y$, and $x-y$ directions. The long direction of the ladder is oriented along the x axis (for the five-orbitals results, the long direction is the y axis, thus a rotation was carried out). "123 compound" column: hopping parameters obtained from tight-binding fits to the band calculations for $BaFe_2Se_3$ presented in the section of the five-orbital Hubbard model. As explained in the five-orbitals section the fully Hermitian matrix is obtained by constructing 4×4 matrices using the transpose of the 2×2 matrices here provided. "DMRG hoppings" column: resulting hopping set for a two-orbital model with one iron atom per unit cell used in the actual DMRG calculations for the 123-ladder compound. In this case all of the hopping matrices are Hermitian already for the 2×2 cases.

Matrix	123 compound	DMRG hoppings
t^x	$\begin{pmatrix} 0.14769 & -0.05309 \\ 0.05309 & 0.27328 \end{pmatrix}$	$\begin{pmatrix} 0.14769 & 0 \\ 0 & 0.27328 \end{pmatrix}$
t^y	$\begin{pmatrix} 0.28805 & 0.01152 \\ 0.01152 & 0.00581 \end{pmatrix}$	$\begin{pmatrix} 0.28805 & 0.01152 \\ 0.01152 & 0.00581 \end{pmatrix}$
t^{x+y}	$\begin{pmatrix} -0.21166 & -0.08014 \\ -0.08430 & -0.18230 \end{pmatrix}$	$\begin{pmatrix} -0.21166 & -0.08430 \\ -0.08430 & -0.18230 \end{pmatrix}$
t^{x-y}	$\begin{pmatrix} -0.21166 & 0.08014 \\ 0.08430 & -0.18230 \end{pmatrix}$	$\begin{pmatrix} -0.21166 & 0.08430 \\ 0.08430 & -0.18230 \end{pmatrix}$

dominates, as in the Lanczos calculations. Overall, the DMRG and Lanczos results are in qualitative agreement, showing that the CX state and block-AFM state reported experimentally are stable in portions of the phase diagram of the two-orbital Hubbard model with the FeAs hoppings, while other states such as CY and FM (not shown) are close in energy.

C. Selenides hoppings for the two-orbitals model

As explained before, the DMRG results shown above in Fig. 5 for the two-orbital Hubbard model were obtained by using the hopping parameters originally developed for pnictide compounds. As also addressed for the case of the five-orbital Hubbard model, this is a crude approximation for $BaFe_2Se_3$ because the hopping parameters are material dependent making a study of the two-orbital Hubbard model with a set of hoppings corresponding to the true 123-ladder selenide compound imperative. This more realistic set of parameters was obtained by fitting tight-binding models to the band structure first-principles results discussed in Sec. II in the context of the five-orbital Hubbard model. Letting $t^{\alpha}_{\gamma,\gamma'}$ be the hopping matrix defined in the orbital space $\gamma = \{d_{xz}, d_{yz}\}$ along the $\alpha = x, y, x+y,$ and $x-y$ directions between nearest and next-nearest iron atoms, the set of hoppings for two orbitals can be obtained, and they are shown in the second column of Table II ("123 compound" column). Note that the five-orbitals results had the long direction along the y axis, but here a rotation was carried out and the long direction is along the x axis.

For the two-leg ladder used in the DMRG calculations, the presence of the Se atoms with a staggered location above and below the FeSe ladders in the 123 material imply that the unit cell must be larger than in the absence of that lattice distortion.[39] The other small lattice distortion along the ladder legs incorporated in the five-orbitals results also demand such an enlarged unit cell. However, this doubling of the unit cell increases the complexity of the DMRG calculation because operators for the additional iron atoms belonging to the enlarged unit cell must be kept. Then, in order to simplify the DMRG computation, approximations (discussed in the next paragraph) will be introduced to reduce the problem to a two-orbital Hubbard model where all Fe-Fe bonds along the leg direction are equivalent. The final set of hoppings used in our DMRG calculation are shown in the "DMRG hoppings" column shown in Table II. They were obtained by averaging hoppings along the same direction but for different bonds.

D. DMRG and selenides hoppings

The results obtained with the DMRG technique applied to the two-orbital Hubbard model using the hoppings for selenides described in the previous subsection are shown in Fig. 6. Technical details are the same as in the case of the pnictides hoppings. Figure 6(a) contains the phase diagram from the wave vectors that dominate in the spin structure factor. Figures 6(b) and 6(c) display the behavior of the spin structure factor at particular couplings, for the two most important states. Similarly as in the case of the hoppings for pnictides, at $n = 2$ there is a dominance of the CX state. In fact, the region of stability of this CX state is larger with the selenides hoppings than with the pnictides hoppings. This may lead to the conclusion that for new ladder compounds synthesized in the future the CX state should be more likely to appear than the block-AFM state. Or it could be that our analysis does not include a lattice distortion that favors the block-AFM state over the CX state.

With regard to the block-AFM state, in Fig. 6(a) it is shown that this phase indeed exists in the regime of hole doping, contrary to the case of the hoppings for pnictides where the block-AFM state was found for electron doping, in a region of approximately the same size in the phase diagram. Not finding this state at precisely $n = 2$ is not a problem since the actual population of the d_{xz} and d_{yz} orbitals is not precisely 2 in the real materials. What is perhaps more surprising is the dominance of the CX state over the block-AFM state, contrary to the results of the five-orbitals model where the latter was fairly stable. This result highlights the shortcomings of the two-orbitals model.

In the phase diagram of Fig. 6 other phases not observed experimentally are found such as the CY state and the FM state, again similar to the case of the hoppings for pnictides or for the five-orbitals models. While the precise location of the phases varies from model to model and depends on the hoppings, the systematic presence of the block-AFM and CX states is clear in our results.

However, as in the case of the pnictides hoppings, it is important to remark that the agreement between five- and two-orbitals calculations is qualitative at best. For instance, consider the case of $n = 2.0$ and $J_H/U = 0.25$ in Fig. 6(a).

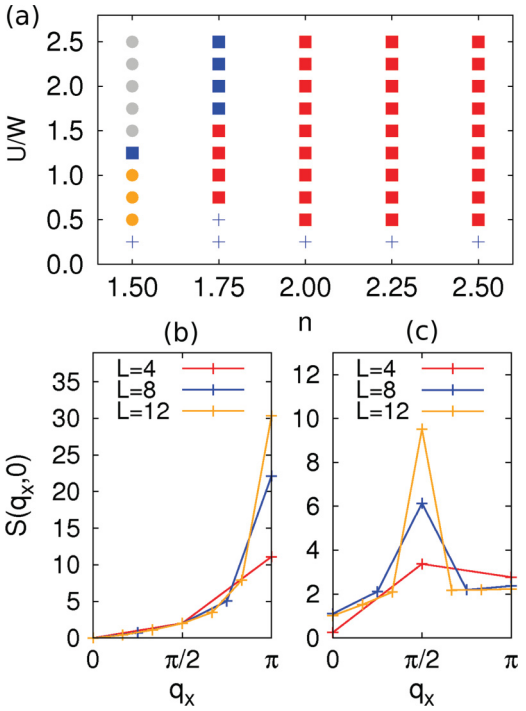

FIG. 6. (Color online) (a) Phase diagram of the two-orbital Hubbard model studied with the DMRG method employing the hopping amplitudes presented in Table II (right column). The cluster used is of size 2×8 with open boundary conditions, and $J_H/U = 0.25$. Shown are results varying U/W and the number of total electrons N as 24, 28, 32 ($n = 2$), 36, and 40. The assignments of the many phases are decided based on the wave vector of the dominant peak in the spin structure factor. The paramagnetic (PM) phase was assigned based on the similarity with the $U = 0$ results, and for this reason the frontier between the PM and magnetic phases may not be precise. The color convention is as in Fig. 4, and 300 states and 15 sweeps were used. (b) DMRG results showing the dominance of the CX state $(\pi,0)$ with increasing L in the spin structure factor $S(q_x,0)$ using $2 \times L$ clusters at $U/W = 1.25$, $J_H/U = 0.25$, and $n = 2$. In these runs, 450 states and 15 sweeps were used. (c) Same as (b) but for the block-AFM state with wave vector $(\pi/2,0)$, at $U/W = 1.25$, $J_H/U = 0.25$, and $n = 1.5$, using 2×4, 2×8, and 2×12 clusters.

Here, as in the case of the pnictides hoppings Fig. 5(a), the CX state dominates in the range of U/W explored. However, for the case of five orbitals at $n = 6.0$ and $J_H/U = 0.25$ in Fig. 3(a), it is the block-AFM state that dominates. Thus, only by including variations in the electronic density n is that similarities between the two cases do emerge.

E. Spin-fermion model results

Complementing these studies, the two-orbital spin-fermion model for the pnictides[22,23] was also analyzed using a 2×16 cluster and Monte Carlo (MC) techniques, employing approximately 50000 MC steps (not shown). At $n \sim 2$ and $J_H \geqslant 0.2$ eV, the CX state was found, while at $n = 2.5$ and a similar range of J_H the block-AFM state was found, in agreement with the Lanczos and DMRG studies.

V. CONCLUSION

Using five- and two-orbital models for the two-leg ladder compounds $BaFe_2Se_3$ and KFe_2Se_3, the phase diagrams of these models were studied using several many-body techniques. The richness of the reported phase diagrams demonstrates that Fe-based superconductors are more complex than early investigations based on Fermi surface nesting ideas anticipated.[2] More specifically, in this study it has been argued that the experimentally observed CX and 2×2 block-AFM states shown in Fig. 1 are indeed the ground state of purely electronic Hubbard models in robust regions of parameter space when varying U/W, J_H, and the electronic density n, at least within the HF approximation. Our effort suggests that to understand the stability of the 2×2 block states, theoretical studies of electronic models using the geometry of two-leg ladders (much simpler than a full two-dimensional layer) may be sufficient, although for a quantitative description quantum fluctuations and the effect of lattice distortions may be needed. Our study also predicts that several other magnetic phases could become stable in the vicinity of the CX and block-AFM states in the phase diagram. The other candidates are in Fig. 1 and the list includes the G-AFM, CY, and FM states, and to a lesser extent the flux and T states. The experimental search for these states via chemical substitution or pressure would be important to improve the interplay between theory and experiments for the Fe-based superconductors. Since these magnetic arrangements are close in energy, glassy behavior caused by a multiplicity of energy minima is also possible.[12] Finally, by comparing results using two sets of hopping amplitudes (one realistic for the ladder selenides and obtained via first-principles calculations, and another borrowed from pnictides investigations), several similarities were unveiled particularly at intermediate and large Hubbard couplings.

ACKNOWLEDGMENTS

The authors thank A. S. Sefat and B. Saparov for useful conversations. This work was supported by the US DOE, Office of Basic Energy Sciences, Materials Sciences and Engineering Division (Q.L, S.L., G.D.S., E.D.), by the National Science Foundation under Grant No. DMR-1104386 (A.N., J. Rincón, A.M.), by CONICET, Argentina (J. Riera), and by the Center for Nanophase Materials Sciences, sponsored by the Scientific User Facilities Division, BES, US DOE (G.A.). L.W. and W.K. acknowledge support by the US Department of Energy, Office of Basic Energy Sciences DE-AC02-98CH10886, DE-FG02-05ER46236, and DOE-CMCSN.

[1] D. C. Johnston, Adv. Phys. **59**, 803 (2010), and references therein.
[2] P. C. Dai, J. P. Hu, and E. Dagotto, Nature Phys. **8**, 709 (2012), and references therein.
[3] E. Dagotto, Rev. Mod. Phys. arXiv:1210.6501.
[4] J. Guo, S. Jin, G. Wang, S. Wang, K. Zhu, T. Zhou, M. He, and X. Chen, Phys. Rev. B **82**, 180520(R) (2010).

[5]W. Bao, Q. Huang, G. F. Chen, M. A. Green, D. M. Wang, J. B. He, X. Q. Wang, and Y. Qiu, Chin. Phys. Lett. **28**, 086104 (2011).
[6]F. Ye, S. Chi, Wei Bao, X. F. Wang, J. J. Ying, X. H. Chen, H. D. Wang, C. H. Dong, and M. H. Fang, Phys. Rev. Lett. **107**, 137003 (2011).
[7]A. Ricci, N. Poccia, G. Campi, B. Joseph, G. Arrighetti, L. Barba, M. Reynolds, M. Burghammer, H. Takeya, Y. Mizuguchi, Y. Takano, M. Colapietro, N. L. Saini, and A. Bianconi, Phys. Rev. B **84**, 060511(R) (2011).
[8]X.-P. Wang, T. Qian, P. Richard, P. Zhang, J. Dong, H.-D. Wang, C.-H. Dong, M.-H. Fang, and H. Ding, Europhys. Lett. **93**, 57001 (2011).
[9]A. Krzton-Maziopa, E. Pomjakushina, V. Pomjakushin, D. Sheptyakov, D. Chernyshov, V. Svitlyk, and K. Conder, J. Phys.: Condens. Matter **23**, 402201 (2011).
[10]J. M. Caron, J. R. Neilson, D. C. Miller, A. Llobet, and T. M. McQueen, Phys. Rev. B **84**, 180409(R) (2011).
[11]H. Lei, H. Ryu, A. I. Frenkel, and C. Petrovic, Phys. Rev. B **84**, 214511 (2011).
[12]$BaFe_{1.8}Se_3$ (i.e., an iron deficient version of the 123 ladders) presents spin-glass behavior and an activation energy $\Delta = 0.30$ eV. See B. Saparov, S. Calder, B. Sipos, H. Cao, S. Chi, D. J. Singh, A. D. Christianson, M. D. Lumsden, and A. S. Sefat, Phys. Rev. B **84**, 245132 (2011).
[13]J. M. Caron, J. R. Neilson, D. C. Miller, K. Arpino, A. Llobet, and T. M. McQueen, Phys. Rev. B **85**, 180405(R) (2012).
[14]Y. Nambu, K. Ohgushi, S. Suzuki, F. Du, M. Avdeev, Y. Uwatoko, K. Munakata, H. Fukazawa, S. Chi, Y. Ueda, and T. J. Sato, Phys. Rev. B **85**, 064413 (2012).
[15]E. Dagotto, J. A. Riera, and D. J. Scalapino, Phys. Rev. **45**, 5744 (1992).
[16]E. Dagotto and T. M. Rice, Science **271**, 5249 (1996).
[17]E. Dagotto, Rep. Prog. Phys. **62**, 1525 (1999).
[18]W. Li, H. Ding, P. Zhang, P. Deng, K. Chang, K. He, S. Ji, L. Wang, X. Ma, J. Wu, J.-P. Hu, Q.-K. Xue, and X. Chen, arXiv:1210.4619.
[19]The results found in this study are compatible with recent first-principles calculations that also reported a block-AFM state for the 123 ladders, see W. Li, C. Setty, X. H. Chen, and J. P. Hu, arXiv:1202.4016.
[20]E. Dagotto, Rev. Mod. Phys. **66**, 763 (1994).
[21]S. R. White, Phys. Rev. Lett. **69**, 2863 (1992); U. Schollwöck, Rev. Mod. Phys. **77**, 259 (2005).
[22]W.-G. Yin, C.-C. Lee, and W. Ku, Phys. Rev. Lett. **105**, 107004 (2010).
[23]S. Liang, G. Alvarez, C. Sen, A. Moreo, and E. Dagotto, Phys. Rev. Lett. **109**, 047001 (2012), and references therein.
[24]Q. L. Luo, G. Martins, D.-X. Yao, M. Daghofer, R. Yu, A. Moreo, and E. Dagotto, Phys. Rev. B **82**, 104508 (2010).
[25]It is well known that the hopping amplitudes change from material to material as shown in T. Miyake, K. Nakamura, R. Arita, and M. Imada, J. Phys. Soc. Jpn. **79**, 044705 (2010).
[26]S. Graser, T. A. Maier, P. J. Hirschfeld, and D. J. Scalapino, New J. Phys. **11**, 025016 (2009).
[27]K. Schwarz, P. Blaha, and G. K. H. Madsen, Comput. Phys. Commun. **147**, 71 (2002).
[28]Wei Ku, H. Rosner, W. E. Pickett, and R. T. Scalettar, Phys. Rev. Lett. **89**, 167204 (2002).
[29]M. Daghofer, A. Nicholson, A. Moreo, and E. Dagotto, Phys. Rev. B **81**, 014511 (2010).
[30]Q. Luo, A. Nicholson, J. A. Riera, D.-X. Yao, A. Moreo, and E. Dagotto, Phys. Rev. B **84**, 140506(R) (2011).
[31]Q. Luo, D.-X. Yao, A. Moreo, and E. Dagotto, Phys. Rev. B **83**, 174513 (2011).
[32]For details see D. D. Johnson, Phys. Rev. B **38**, 12807 (1988) (linear mixing parameter $\alpha = 0.5$).
[33]R. Yu, K. T. Trinh, A. Moreo, M. Daghofer, J. A. Riera, S. Haas, and E. Dagotto, Phys. Rev. B **79**, 104510 (2009).
[34]Y.-Z. Zhang, H. P. Lee, H.-Q. Lin, C.-Q. Wu, H. O. Jeschke, and R. Valenti, Phys. Rev. B **85**, 035123 (2012).
[35]A. Nicholson, W. H. Ge, X. Zhang, J. A. Riera, M. Daghofer, A. M. Oleś, G. B. Martins, A. Moreo, and E. Dagotto, Phys. Rev. Lett. **106**, 217002 (2011).
[36]M. Daghofer, A. Moreo, J. A. Riera, E. Arrigoni, D. J. Scalapino, and E. Dagotto, Phys. Rev. Lett. **101**, 237004 (2008).
[37]A. Moreo, M. Daghofer, J. A. Riera, and E. Dagotto, Phys. Rev. B **79**, 134502 (2009).
[38]Whether a true long-range order or a slow power-law decay in the correlation functions dominates is difficult to establish with the limited L data set available.
[39]For the FeAs layers this staggering is also present, but in the pnictides hoppings used in this paper the effect was ignored (i.e., all the As atoms were assumed to be at the same height with respect to the Fe layer).